Electrochemical Monitoring of Reduction and Binding of Iron Amyloid-β Complexes at Boron-Doped Diamond Electrode

Gang Zhang[1], Zhaohui Huo[2], Yanli Zhou[3], Xiaohua Zhu[2], Hongru Wang[1], Yong Liang[2,*] Maotian Xu[3,*]

[1] College of Resources and Environment, Shanxi University of Science and Technology, Xi'an 710021, People's Republic of China
[2] Department of Chemistry and Environment, South China Normal University, Guangzhou 510631, People's Republic of China
[3] Henan Key Laboratory Cultivation Base of Nanobiological Analytical Chemistry, Department of Chemistry, Shangqiu Normal University, Shangqiu 476000, People's Republic of China
[*]E-mail: liangy@scnu.edu.cn; xumaotian@sqnc.edu.cn

The amino acid residues for reduction and binding of amyloid–β peptide (Aβ)–Fe(III) complexes were investigated mainly by voltammetry at boron-doped diamond electrodes. Distinguished from natural Fe(III)–Aβ(1–16) complex, the recovering redox behavior of Fe(III)–Aβ(Y–F) complex showed higher free-ion concentration and weaker bonding ability, evidencing that Fe(III) primarily binded to Aβ via Tyr10. Whereas, there were no detectable distinctions in electroactivity along with UV/vis absorptivity and fluorescence quenching between Fe(III)–Aβ(1–16) and Fe(III)–Aβ(H–N), which indicates that three His were eliminated in direct bonding to Fe(III). Compared with Fe–Aβ(1–16), the significant enhancement of $I_{p(Fe(II)-Fe(0))}$ in Fe–Aβ(1–42), Fe–Aβ(25–35), and even the exogenous Met to Fe(III) provided electrochemical evidences that the reduction of Fe(III) to Fe(II) was aroused by Met directly. Zn(II) which was redox-silent, also contributed the pathogenesis but can not affect the redox signal of Fe(III)–Aβ.

1. INTRODUCTION

Two of the characteristic pathologic features in the brains of Alzheimer's disease (AD) patients are the deposition of aggregated amyloid–β peptide (Aβ) and the high levels of oxidative stress [1]. Both these phenomena are related to the interactions of Aβ with metal ions such as zinc, copper, and iron [2]. When Aβ bonds the above metal ions, the peptide aggregates, and then reactive oxygen species (ROS) are generated when the metals including copper and iron are redox active. The interactional mechanism of Aβ and copper has been widely reported. Considering that Fe(III) is an

even stronger oxidant with higher concentration in Aβ deposits than Cu(II) [3,4], the possible binding sites and redox sites may be different from those of Cu(II). Meanwhile, the paucity of references about Fe–Aβ complexes heightens the demand to understand the contribution of iron in the pathomechanism of AD.

Reducing efficiency of peroxide production in Fe(III)-rat Aβ suggests that at least one of Tyr10 and His13 is crucial in the peroxide-mediated neurotoxicity of human Aβ, because charged Arg5 is unlikely to bind to iron [5-7]. In addition, contradictory reports existed in the identity of electron donor of Met35 side chain [8-12], potentially, as differences with the handling of Aβ and/or differences in the solution conditions (i.e. pH, buffer, concentrations, and type of peptide) were used in the various studies [13,14]. Therefore, the reduction and binding of iron–Aβ complex is worth exploring.

Owing to the similarity of electrochemical and biological reactions, electrochemical methods can simulate the redox mechanism of organisms. It can allow for the accurate and direct determination of potentials and currents of redox–active biomolecules, and provide insight about electron transfer (ET) reactions to get more informations [15,16]. Boron-doped diamond (BDD) thin films have emerged as attractive new electrode materials because of their good electrochemical properties including biocompatible, wide electrochemical potential window, very low double-layer capacitance, extreme electrochemical stability and high resistance to deactivation by fouling. The advantages and supremacy of the BDD electrode over the traditional electrodes such as, glassy carbon (GC) and gold electrodes, make it a real electrode for the determination of the redox behavior reliably for biomolecules, and is expected to achieve facile ET rates at the electrode/solution interface [17-19].

Herein, the interaction mechanisms of Aβ–Fe(III) complexes involving the amino acid residues in Aβ for reduction and binding were studied. The Fe/Tyr or Fe/His binding hypothesis was investigated using Aβ(1−16) with Tyr10 substituted with Phe or His residues replaced by Asn. The effect of redox-silent zinc for electrochemical behavior of the interaction of Aβ–Fe was also discussed.

2. EXPERIMENTAL PART

2.1. Reagents and Materials

Aβ(1−16), Aβ(25−35), Aβ(1−42), and mutant Aβ were purchased from the Chinese Peptide Co. (Hangzhou, China). Aβ peptide need special pretreatment and preservation [17]. Other chemicals were of analytical grade and obtained from Aladdin Co. (China). All the aqueous solutions were prepared using deionized water (Millipore, > 18 MΩ cm). $FeCl_3$ was used fresh on the same day. The pretreatment and storage of Aβ peptide refer to the supporting information. Not specified, all the Aβ–Fe complexes were incubated at 37 °C for 1.5 h in constant temperature incubation box.

Studies using analogues of Aβ(1−16) in which all of His residues have been replaced by Asn or in which Tyr residue has been substituted for Phe are followed.

Designation   Sequence

Aβ(1−16):   DAEFRHDSGYEVHHQK

Aβ(H–N) :   DAEFRNDSGYEVNNQK

Aβ(Y–F):   DAEFRHDSGFEVHHQK

Aβ(25–35):   GSNKGAIIGLM

Aβ(1–42):   DAEFRHDSGYEVHHQKLVFFAEDVGSNKGAIIGLMVGGVVIA

2.2. Preparation of BDD thin films

BDD thin films were deposited by hot-filament chemical vapor depostion on silicon (100) wafers. The silicon substrates were abraded with 1 μM diamond powder for 15 min prior to deposition, after which they were ultra-sonically cleaned successively in acetone and in deionized water for 1 min. Acetone were used as a carbon source at the flow rate of 50 mL min^{-1}, while trimethyl borate dissolved in the acetone was used as boron source at a B/Cmolar ratio of 0.5%. High-purity hydrogen (99.99%) at the flow rate of 200 mL min^{-1} was used as the carrier gas. The Ta filament with the diameter of 0.6 mm and the length of 14 cm was used as hot–filament, and the filament-substrate distance was 6 mm. The deposition of the film was carried out at the vapor pressure of 1.7 kPa, and a BDD film with the thickness of 20.0 μm was achieved after 7 h of deposition.

2.3. Instrumentation

Cyclic voltammograms (CV) and differential pulse voltammetry (DPV) measurements were performed on a CHI660D electrochemical workstation (Shanghai, China) in a three-electrode cell system with a BDD electrode, a platinum wire (CHI, China) and an Ag/AgCl electrode (CHI, China) as the working electrode, auxiliary electrode, and reference electrode, respectively. Before use, the BDD electrodes were sonicated successively in 2-propanol and deionized water for 15 min. Unless otherwise stated, KCl (0.2 M) in deionized water was used as the supporting electrolyte solution. In CV experiments, scan rate was 0.05 Vs^{-1}. All the electrochemical experiments were carried out at room temperature.

AFM (Agilent 5500, Agilent Technologies, USA) samples were deposited on mica substrates which were firstly deposited and adsorbed nickel salt for 5 minutes, then rinsed twice with 200 μL deionized water, and finally dried up with a weak flow of N_2 gas for 1 min. All AFM experimental data were collected in tapping mode in air at optimal force, and all the operations were done in an automated moisture control box with 30–40% humidity at room temperature.

UV/vis spectrum (Hitachi, UV2300) were recorded by adding aliquots of Fe(III) to the cuvette containing a known initial concentration of peptide in 1.0 cm quartz cells at room temperature. Fuorescence measurements of Aβ peptide solutions were carried out on a flurescence spectrophotometer (Cary Eclipse, USA) with 280 nm excitation wavelength and 3 nm widths for the entrance and exit slits.

3. RESULTS AND DISCUSSION

3.1. AFM characterization on Aβ aggregation

AFM is able to capture nm-scale structures adsorbed onto the surface, and is effectively used to monitor the aggregative morphology of biomacromolecules [20]. Fig. 1 shows the effect of Fe(III) on the aggregation morphology of Aβ(1–16) and Aβ(1–42). Fresh hydrophilic Aβ(1–16) did not aggregate, and the average z-height was less than 2 nm. Hydrophobic Aβ(1–42) formed slightly dot aggregation (z-height ~ 12 nm). When Fe(III) was incubated with Aβ(1–16), much denser aggregates with spherical or nonfibrillar "amorphous" deposits were observed on the mica surface (Fig. 1B). If substituted by Aβ(1–42), in which case fibrillar and banding shape deposits were found (Fig. 1D). According to the AFM analysis of immobilized seeds, the average z-heights were in the range of ~20 nm and ~11 nm for Aβ(1–16) and Aβ(1–42) in the presence of Fe(III), respectively. These observations suggested that Fe(III) could be one of the key mediating factors for the formation of fibrillar β-sheet amyloid deposition.
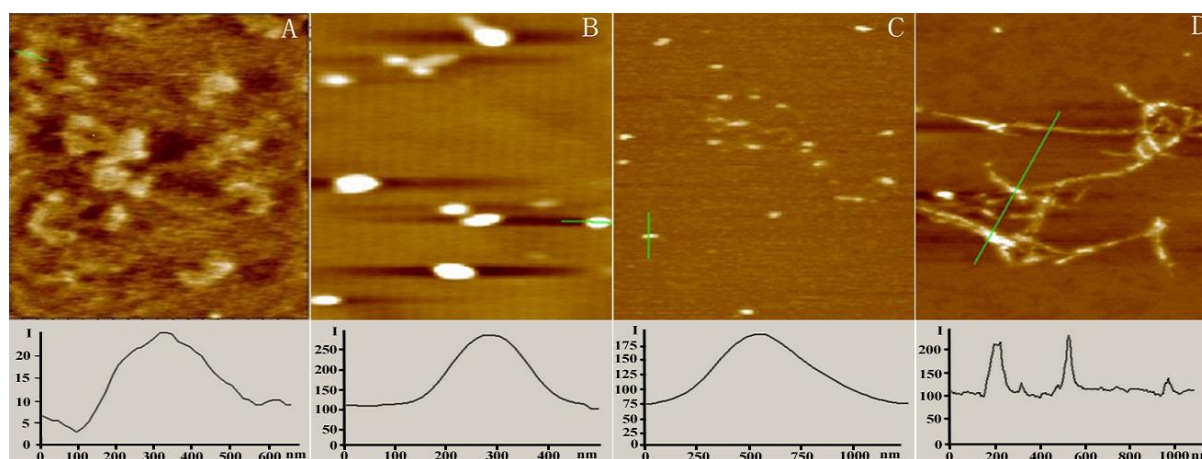

Figure 1. Tapping mode AFM images of Aβ(1–16) and Aβ(1–42) deposits in the absence or presence of Fe(III). The deposits were obtained by incubating freshly prepared Aβ(1–16) (5.0 μM) in 0.2 M KCl containing 5% Me$_2$SO (v/v) (A) without metal ion, and (B) with 100.0 μM Fe(III) at 37 °C for 1.5 h. (C) and (D) were the same as (A) and (B) except that the Aβ(1–16) was replaced with Aβ(1–42) at the same concentration. The size of each AFM image was 4 μm × 4 μm.

3.2. Electrochemical properties of Fe(III)–Aβ complexes

Phosphate buffer solution (PBS) may represent a more "physiological" uffering system, while the intensity of Fe(III)/Fe(II) reduction current decreased and iron ions formed sediment in the PBS. Since the solubility of Fe(III) in water is very low at neutral pH owing to hydrolysis of the metal ion [21], most Fe(III) ions are expected to be in precipitates as hydroxy compounds. To increase the solubility of the Fe(III) ion and the binding capacity with Aβ in the solution phase, the mixture of Fe(III) and Aβ were prepared at 0.2 M KCl solution conditions. The mixed solution was weak acidic (pH 6.0), where hydroxy compounds were less produced.

Voltammetry is an outstanding method to the monitor subtle changes in redox properties of the electroactive species and reflect their interactions. Electrochemical consequences of Fe(III) ability to interact with Aβ were observed based on CV and DPV. They follow the changes of the Fe(III)-related electrode processes in the absence and presence of Aβ, and the results are presented in Fig. 3, Fig. 4 and Fig. 5. Aβ(1–16) corresponds to the N–terminal hydrophilic segment of full-length Aβ and this segment contains potential metal binding sites: three histidines (His6, 13 and 14) and one tyrosine (Tyr10) [8]. To explore the role of Met35, Aβ(25–35) is a generally accepted model. Thus, Aβ(1–42), two fragments including Aβ(1–16) and Aβ(25–35), and site-directecd mutants of Aβ(1–16) (Aβ(Y–F) and Aβ(H–N)) have been selected.
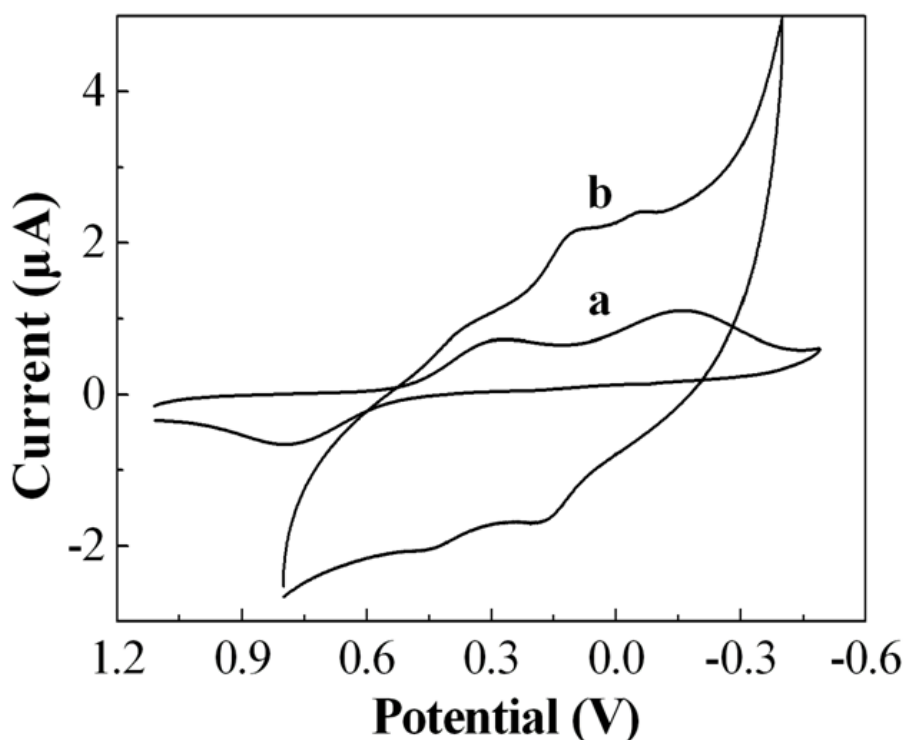

Figure 2. CVs of 100.0 μM Fe(III) in 0.2 M KCl at the BDD (a) and GC (b) electrode.

Two well-defined reduction peaks of 100.0 μM Fe(III) at BDD electrode (Fig. 2, curve a) were observed with low background currents at 0.288 V for the reduction of Fe(III) to Fe(II) and at –0.165 V for the reduction of Fe(II) to Fe(I), which were substantially superior to the weak signals at GC electrode (curve b). The above outstanding electrochemical properties showed that the BDD electrode owned the potential high performance for the further study of Aβ–Fe(III) complexes. Deduced from DPV (Fig. 3), peak current at ~ –0.313 V of CV (Fig. 4) was assigned to the reduction of Fe(II)–Aβ to Fe(0)–Aβ. The results demonstrated that complexation of Aβ with Fe(III) altered the secondary structure near the N-terminus and further made Fe(III) centers less accessible to electrochemical reduction.
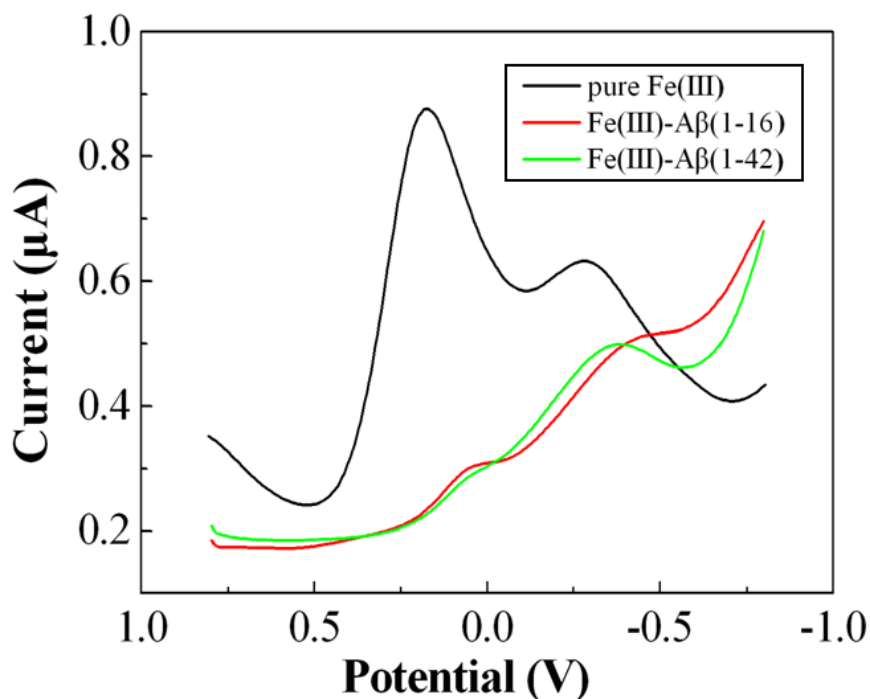
Figure 3. DPVs of 100.0 µM Fe(III) without Aβ, with 10 µM Aβ(1–16) and 10 µM Aβ(1–42) in 0.2 M KCl containing 5% Me$_2$SO (v/v).
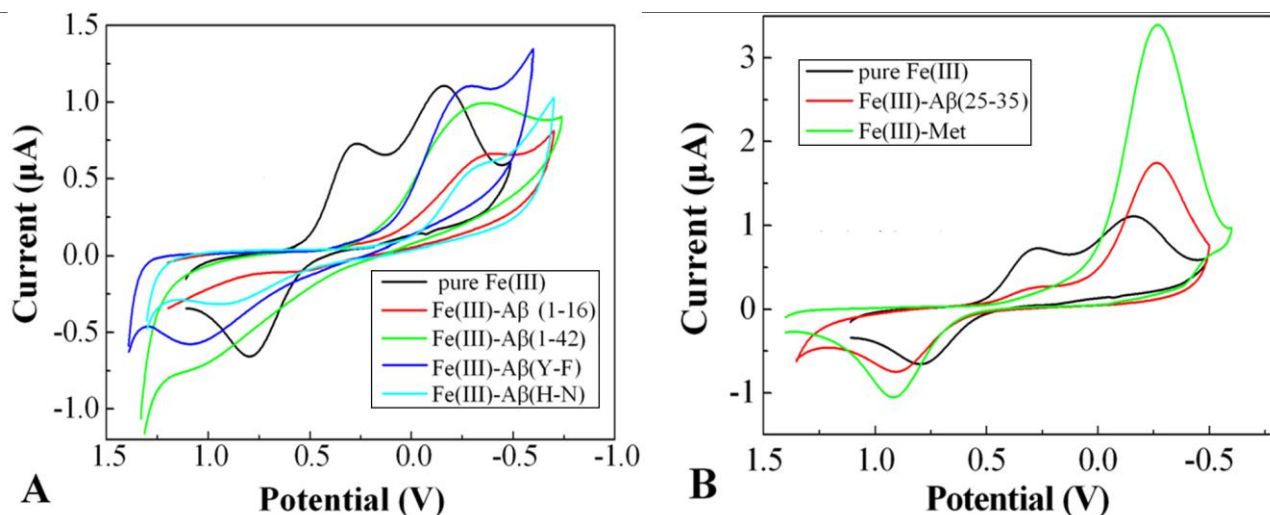

Figure 4. CVs of 100.0 µM Fe(III) before and after the addition of 10.0 µM different Aβ segments in 0.2 M KCl containing 5% Me$_2$SO (v/v). (A): without Aβ, with Aβ(1–16), Aβ(1–42), Aβ(H–N), and Aβ(Y–F). (B): without Aβ, with Aβ(25–35), and Met.

As Aβ(1–42) was more prone to aggregation and caused more significant adsorption onto the electrode surface, Fe–Aβ(1–42) was expected to have a smaller diffusion coefficient and led to a smaller reduction current than Fe–Aβ(1–16). It should be pointed out that, the current of Fe(II)–Aβ(1–42)/Fe(0)–Aβ(1–42) at ~ –0.313 V was higher than that of Fe(II)–Aβ(1–16) /Fe(0)–Aβ(1–16) evidently (Fig. 3). To further explore this phenomenon, CV of Aβ(25–35) in the presence of Fe(III) was

investigated under the same experimental conditions (Fig. 4B). The increase of the current of Fe(II)–Aβ(25–35)/Fe(0)–Aβ(25–35) vis Fe(II)–Aβ(1–16)/Fe(0)–Aβ(1–16) and the above enhancive current of Aβ(1–42) complex vis Aβ(1–16) complex could prove the increase of Fe(II) concentration.

In Fig. 4B, stronger proof of more than a two fold increase in the current of Fe(II)/Fe(0) after adding exogenous Met to Fe(III) had confirmed oxidation ability of Met35. Oxidative stress and ROS generated by this are characteristic pathologic features present in the brains of AD [22-24]. As to examine the potential redox ligands on Aβ for Fe(III), the intrinsic redox properties of Fe(III) provide an important tool for a better understanding of the valence conversion. Met was one of the most easily oxidized amino acids and in AD brain, and the oxidation product of methionine sulfoxide was detected. [25-27].The secondary structure of the C-terminal region of Aβ(1–42) is also predicted to contribute to the Met–associated oxidative stress. The backbone carbonyl or Ile31, within a van der Waals distance of the S-atom of Met35, primed the lone pairs of electrons on the S-atom of Met35 for oxidation. That is to say, one-electron could be easily removed. That is unique about human Aβ(1–42) to undergo Met-based chemistry [28, 29]. Met really plays a key role in the redox mediated toxicity of Aβ.

Superimposed CVs in Fig. 4A are the voltammograms of Fe(III) with natural Aβ(1–16), Aβ(1–42) and mutant Aβ(1–16) (Aβ(H–N) and Aβ(Y–F)). Inhibitory effect which decreased the peak current of iron ions in the presence of Aβ(1–16) was observed during reduction. Complexation of Fe(III) with Aβ(1–16) resulted in diminished concentration of electroactive ions. Meanwhile, mutations of these metal-binding ligands substantially altered the coordination and complexing properties of the proteins. Differing from the human Aβ, at two potential metal binding sites, viz. His13 and Tyr10, mice did not develop AD, which may be attributed to the pale binding competitiveness of mice Aβ. In the case of familial AD, Aβ was point mutated, but none of the mutations occurs in the metal binding region. As shown in Fig. 4A, when the same ratio of Aβ was used, the rank order of inhibitory effect, which decreased the electrochemical activity, was Aβ(1–16) ≈ Aβ(H–N) > Aβ(Y–F). Marked difference in the redox activity was obtained between Fe(III) and Aβ segments including or excluding Tyr10 residues and iron ions confined by Aβ(Y–F) were subdued. Further, the lower concentration of Fe(II)–Aβ(Y–F) than Fe(II)–Aβ(1–16) ($I_{(Fe(II)–Aβ(Y–F)/Fe(0)–Aβ(Y–F))} < I_{(Fe(II)–Aβ(1–16)/Fe0)–Aβ(1–16))}$) rejected the possibility of Tyr10 as an oxidant. To conclude, Tyr10 could coordinate with Fe(III) directly, however, Tyr10 could not reduced Fe(III). Inversely, there was no apparent diversity for His residues, as a result His was likely to be excluded in direct coordination to Fe(III). These results are in sharp contrast to Zn(II)– or Cu(II)–induced aggregation of Aβ, in which His residues act as the primary metal binding sites. Zinc which is redox-silent, also contribute the pathogenesis. However, with background subtraction, CVs of Fe–Aβ(1–16) showed little or no change after the addition of Zn(II) (Fig. 5). The first Zn–binding site of Aβ is located in the N–terminal part. The involvement of His 6, 13, and 14 has been suggested as metal-binding ligands in most studies. The binding constant of Fe(III) (K_d ≈10^{-13}~10^{-11} M) to the Aβ is more higher than Zn(II) (K_d of high–affinity Zn(II) binding is ≈ 100 nM, and for low–affinity binding is ≈ 5 μM) [30]. Considering Zn(II) has different binding sites and lower bonding affinity compared with Fe(III), the addition of Zn(II) make no difference for Fe(III)–Aβ(1–16) in our CV.
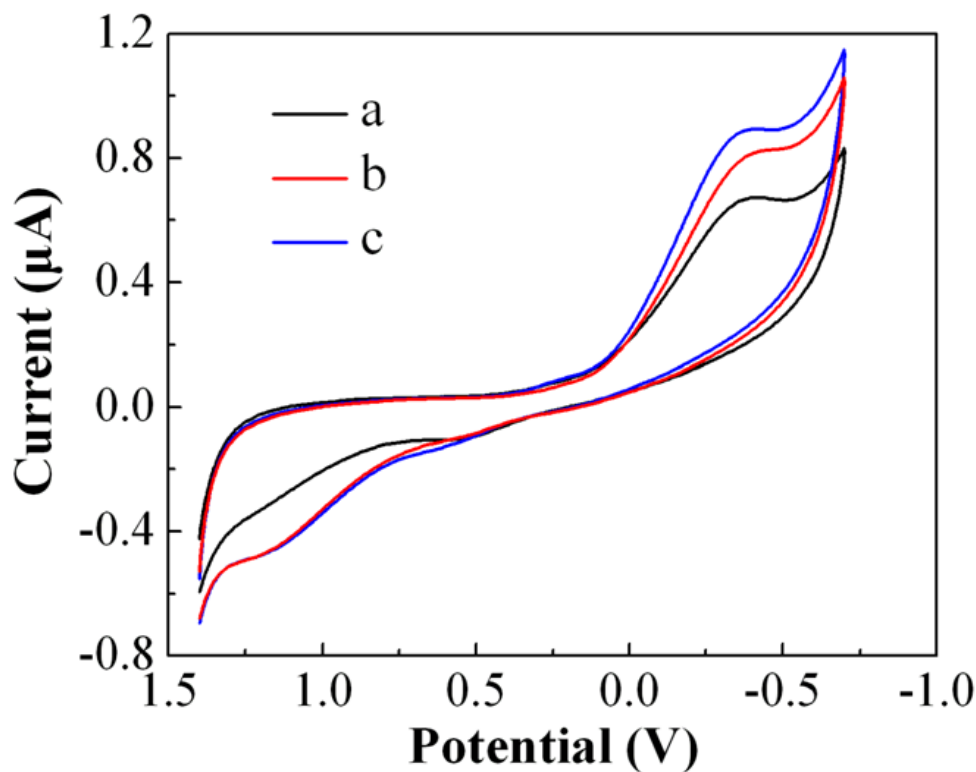
Figure 5. CVs of 10.0 μM Aβ(1−16) in 0.2 M KCl containing 5% Me$_2$SO (v/v) incubated with 100.0 μM Fe(III) for 1.5 h (**a**), with both 100.0 μM Fe(III) and 100.0 μM Zn(II) for 1.5 h (**b**) and firstly with 100.0 μM Zn(II) for 5 h then with 100.0 μM Fe(III) for 1.5h (**c**).

3.3. Spectroscopy characterization of Fe(III)–Aβ complexes

Tyr which has three important components: a carboxylic group, an amino group and a phenolic group, is one of three amino acids with a bulky, uncharged and aromatic side group. Thus, Tyr has an absorption spectrum [31] and a strong fluorescene signal [32], which could be used to detect the binding of Aβ with other molecules. To further verify the effect of three His residues on the Fe(III)−Aβ complex, absorption spectra and fluorescence spectra of natural Aβ(1−16) and mutant Aβ(H–N) after adding different concentrations of Fe(III) were studied. As shown in Fig. 6A and Fig. 6B, a significant decline in the absorbance of Aβ(1−16) at 275 nm was observed upon Fe(III) binding, and the enhancement of the absorption at ~340 nm was accompanied. These changes could be attributed to ligand-to-metal charge transfer processes [33]. The absorbance of Fe(III)−Aβ(H–N) was indistinguishable from Fe(III)−Aβ(1−16), so the removal of the three His residues could not reduce the affinity of Fe(III) with Aβ(1−16). Hence His were not implicated in the binding of Fe(III) to Aβ. In Fig. 6C, upon the addition of Fe(III), the natural Aβ(1−16) and mutant Aβ(H–N) were strongly quenched (≈60% at 1 equiv of Fe(III)) (Fig. 6C). Both of the spectroscopies confirmed that His residues did not induce an appreciable binding or conformational change for Fe(III)−Aβ, which were in accord with the electrochemical characterization at mildly acidic pH. Thus, the N$_τ$ atoms of His were not implicated to coordinate iron as the N ligand.
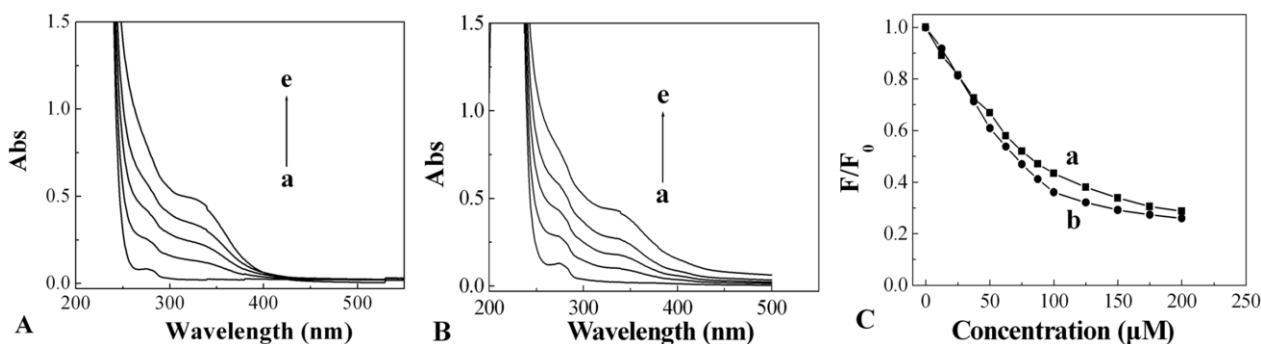
Figure 6. Intensity of Aβ(1–16) (A) and Aβ(H–N) (B) absorption spectra as a function of added Fe(III), (a–e) c(Fe(III)): 0.0, 50.0, 100.0, 150.0 and 200.0 μM, respectively; (C) Intensity of Aβ(1–16) (**a**) and Aβ(H–N) (**b**) fluorescence as a function of added Fe(III). c(Aβ(1–16)) = 50.0 μM and c(Aβ(H–N)) = 50.0 μM in 0.2 M KCl containing 5% Me$_2$SO (v/v). F$_0$ and F are the fluorescence intensities before and after the addition of Fe(III), respectively.

4. CONCLUSIONS

The present study has investigated, for the first time, the interaction of Aβ with Fe(III) mainly by the electrochemical method based on the BDD electrode. Fe(III) bound to Aβ and induced significant aggregation of the peptide. The aggregation morphology of Fe(III)–Aβ(1–16) was spherical and nonfibrillar, which was completely different from the fibrillar shape for Fe(III)–Aβ(1–42) in the AFM images. The CV results of Fe(III)–Aβ(1–42) and Fe(III)–Aβ(25–35) even the exogenous Met to Fe(III) afforded direct electrochemistry evidences for the change of the oxidation state of Fe(III). This study provided effective proof that Met35 involved in the redox chemistry as a reducing agent. The Fe(III)–Aβ complexes showed weaker binding ability when Tyr residue was substituted, evidencing that Fe(III) primarily binds to Aβ via Tyr10. On the other hand, three His residues did not directly be involved in binding. These results were in sharp contrast to Zn(II)– or Cu(II)–induced aggregation of Aβ, in which His residues acted as the primary metal binding sites. The above results of Fe(III)–Aβ interactions may be one of the hinges of the whole molecular mechanism of AD. The other molecular mechanism of AD is doubtless a real challenge in the future work because AD has become the leading neurodegenerative disorder. Additionally, the BDD thin films with outstanding electrochemical properties and inherent biocompatilibility can be used as a real electrode material for the study of bioelectrochemistry.

References

1. J. S. Choi, J. J. Braymer, R. P. Nanga, A. Ramamoorthy and M. H. Lim, *Proc. Natl. Acad. Sci. USA*, 10 (2010) 21990.

2. C. K. Wang, J. Wang, D. J. Liu and Z. X. Wang, *Talanta*, 80 (2010) 1626.
3. M. A. Lovell, J. D. Robertson, W. J. Teesdale, J. L. Campbell and W. R. Markesbery, *J. Neurosci. Meth.*, 158 (1998) 47.
4. A. S. DeToma, J. S. Choi, J. J. Braymer and M. H. Lim, *ChemBioChem,* 12 (2011) 1198.
5. B. D. Shivers, C. Hilbich, G. Multhaup, M. Salbaum, K. Beyreuther and P. H. Seeburg, *EMBO J.,* 7 (1988) 1365.
6. T. Miura, K. Suzuki and H. Takeuchi, *J. Mol. Struct.*, 598 (2001) 79.
7. M. Nakamura, N. Shishido, A. Nunomura, M. A. Smith, G. Perry, Y. Hayashi, K. Nakayama and T. Hayashi, *Biochemistry,* 46 (2007) 12737.
8. K. Watanabe, C. Ishikawa, H. Kuwahara, K. Sato, S. Komuro, T. Nakagawa, N. Nomura, S. Watanabe and M. Yabuki, *Anal. Bioanal. Chem.*, 402 (2012) 2033.
9. S. W. Snyder, U. S. Ladror, W. S. Wade, G. T. Wang, L. W. Barrett, E. D. Matayoshi, H. J. Huffaker, G. A. Krafft and T. F. Holzman, *Biophy. J.*, 67 (1994) 1216.
10. C. Schöneich, *Arch. Biochem. Biophys.,* 397 (2002) 370.
11. S. Varadarajan, J. Kanski, M. Aksenova, C. Lauderback and D. A. Butterfield, *J. Am. Chem. Soc.,* 123 (2001) 5625.
12. M. Palmblad, A. Westlind-Danielsson and J. Bergquist, *J. Biol. Chem.,* 277 (2002) 19506.
13. G. F. Silva, V. Lykourinou, A. Angerhofer and L. J. Ming, *Biochim. Biophys. Acta.,* 1792 (2009) 49.
14. M. Chikae, T. Fukuda, K. Kerman, K. Idegami, Y. Miura and E. Tamiya, *Bioelectrochemistry,* 74 (2008) 118.
15. Z. A. Mangombo, P. Baker, E. Iwuoha and D. Key, *Microchim Acta,* 170 (2010) 267.
16. A. W. Bott, *Curr. Sep.,* 18 (1999) 47.
17. Y. L. Zhou, Z. H. Huo, X. Zhu, X. H. Zhu, M. T. Xu and Y. Liang, *Int. J. Electrochem. Sci.,* 7 (2012) 3089.
18. T. A. Enache and A. M. Oliveira-Brett, *Bioelectrochemistry*, 81 (2011) 46.
19. A. Kraft, *Int. J. Electrochem. Sci.*, 2 (2007) 355.
20. Z. Y. Wu, S. Thiagarajan, S. M. Chen, K. C. Lin, *Int. J. Electrochem. Sci.,* 7 (2012) 1230.
21. L. Svennerholm and C. G. Gottfries, *J. Neurochem.,* 62 (1994) 1039.
22. S. Varadarajan, S. Yatin, M. Aksenova and D. A. Butterfield, *J. Struct. Biol.*, 130 (2000) 184.
23. J. Dong, C. S. Atwood, V. E. Anderson, S. L. Siedlak, M. A. Smith, G. Perry and P. R. Carey, *Biochemistry,* 42 (2003) 2768.
24. J. Wu, A. Wang, Z. Min, Y. J. Xiong, Q. Y. Yan, J. P. Zhang, J. Xu and S. M. Zhang, *Biochem. Biophy. Res. Commn.,* 408 (2011) 382.
25. M. Suazo, C. Hodar, C. Morgan, W. Cerpa, V. Cambiazo, N. C. Inestrosa and M. Gonzalez, *Biochem. Biophy. Res. Commn.,* 382 (2009) 740.
26. Y. W. Kuo, T. A. Kokjohn, T. G. Beach, L. I. Sue, D. Brune, J. C. Lopez, W. M. Kalback, D. Abramowski, C. Sturchler-Pierrat, M. Staufenbiel and A. E. Roher, *J. Biol. Chem.,* 276 (2001) 12991.
27. J. Näslund, A. Schierhorn, U. Hellman, L. Lannfelt, A. D. Roses, L. O. Tjernberg, J. Silberring, S. E. Gandy and B. Winblad, *Proc. Natl. Acad. Sci. USA*, 91 (1994) 8378.
28. M. Coles, W. Bicknell, A. A. Watson, D. P. Fairlie and D. J. Craik, *Biochemistry*, 37 (1998) 11064.
29. Y. Gong, L. Chang, K. L. Viola, P. N. Lacor, M. P. Lambert, C. E. Finch, G. A. Krafft and W. L. Klein, *Proc. Natl. Acad. Sci. USA,*100 (2003) 10417.
30. A. I. Bush, *Neurobiol. Aging,* 23 (2002) 1031.
31. L. Wang, C. S. Ma, X. L. Zhang, Y. B. Ren and Y. Yu, *Fresenius J. Anal. Chem.* 351 (1995) 689.
32. L. Guilloreau, L. Damian, Y. Coppel, H. Mazarguil, M. Winterhalter and P. Faller, *J. Biol. Inorg. Chem.* 11 (2006) 1024.

33. N. C. Maiti, D. L. Jiang, A. J. Wain, S. Patel, K. L. Dinh and F. M. Zhou, *J. Phys. Chem. B,* 112 (2008) 8406.